Nonintrusive characterization of the azimuthal drift current in a coaxial E×B discharge plasma

Cliff A. Thomas, Nicolas Gascon, and Mark A. Cappelli
Stanford University, Stanford, California 94305-3032, USA
(Received 27 May 2006; published 15 November 2006)

A diagnostic is developed for the nonintrusive study of the azimuthal drift current in the coaxial **E**×**B** discharge of a Hall plasma accelerator. The technique of fast current interruption is used to generate a signal on several loop antenna that circle the outer wall of the discharge channel. The signal on the antenna is recorded, and used to determine the spatial distribution of the azimuthal drift at the moment of current interruption. The results of the experiment are compared to estimates derived via prior intrusive measurements, and the intrusive estimates are found to predict the spatial characteristics of the azimuthal drift, but underestimate its total magnitude. The self-induced magnetic field is then calculated and added to the applied magnetic field. The peak total magnetic field is seen to shift 2–5 mm towards the anode due to self-induction, and suffer a reduction in magnitude of 10%–15%. The peak in the total magnetic field is then found to more closely coincide with the peak of the measured electric field than the peak of the vacuum magnetic field. It is concluded that the self-induced magnetic field could be important to anomalous electron mobility in the Hall-effect thruster, and simulation efforts should try to include its impact.

DOI: 10.1103/PhysRevE.74.056402 PACS number(s): 52.70.−m, 52.75.Di, 52.25.Xz

I. INTRODUCTION

The closed-drift Hall plasma accelerator, or Hall-effect thruster (HET), has been in use since the early 1970s for high specific impulse satellite propulsion [1]. In a typical HET the discharge is established across an externally applied magnetic field, **B**, which is sized to confine electrons but not ions. As a result, an electrostatic field arising from the inhibited electron flow, **E**, accelerates ions to high velocity (on the order of 10^4 m/s for a 200 V Xenon HET). The discharge is coaxial so electrons can execute closed-drift motion in the azimuthal direction (**E**×**B**), and cross-field electron diffusion provides current closure. An external hollow cathode neutralizes the space charge of the resulting ion beam (see Fig. 1).

The Hall-effect thruster has received considerable attention not only for its conversion efficiency between electric potential energy and ion kinetic energy, but also for its "anomalous" cross-field electron mobility, a property evident in some of the first studies of these devices [2]. Classical diffusion theory (which scales as B^{-2}) severely underpredicts the cross-field transport in the HET, and numerical models of the discharge must commonly invoke an anomalous diffusion coefficient (like that of Bohm, varying as B^{-1}) to achieve acceptable results [3].

An analysis by Fife [4] of experimental data presented in the Russian literature [5], and recent measurements completed at Stanford University [6,7], both indicate the electron mobility, which is proportional to the inverse Hall parameter, $(\omega\tau)^{-1}$, is a strong function of position. In some portions of the discharge the measured inverse Hall parameter is close to the value given in Bohm's work [8], $(\omega\tau)^{-1}=16$. However, in those regions where the magnetic field is strongest, the mobility is found to approach the value expected for classical diffusion. The origins of this complex electron flow are still debated [9–11], but in parallel, questions arise as to the accuracy of these measurements. The studies cited had to rely primarily on intrusive diagnostics known to perturb the HET plasma, and on measurements of the magnetic field performed in the absence of a discharge. They did not account for the contribution of a self-induced magnetic field. In the present paper we address these two issues by developing a diagnostic that allows the nonintrusive measurement of the longitudinal and radial distribution of the azimuthal drift current, and by calculating the magnetic field induced by this current. It is found that the self-induced magnetic field (though relatively small) could be important to anomalous electron transport in the HET.

II. EXPERIMENTS AND NUMERICAL MODELING

A. Hall discharge and vacuum facility

The plasma source used in this study, the Stanford Hall Thruster (SHT), see Fig. 1, is designed so the measurement of its plasma properties is relatively easy: plasma density, electron energy, ion velocity, etc. [6]. The discharge chamber consists of an annular alumina channel 90 mm in diameter, 11 mm in width, and 80 mm in length. The magnetic circuit consists of four outer coils, one inner coil, and three iron plates that provide a radial magnetic field whose peak in vacuum is 2 mm from the exit plane. A hollow stainless steel ring with 32 equidistant holes (0.5 mm in diameter) serves as the anode and propellant distributor. A commercially available hollow cathode (Ion Tech HCN-252) provides the electron current necessary to sustain the discharge. Further details on the SHT can be found in Ref. [6].

Experiments with the SHT are performed in a 4 m^3 stainless steel vacuum chamber at a pressure of 1×10^{-4} Pa during nominal discharge operation (2 mg/s anode xenon flow, 0.3 mg/s cathode xenon flow, and 500 W discharge power). This is accomplished using a cryogenic pumping system (CVI model number TM1200) with liquid nitrogen shroud. Separate power supplies are used for the discharge, cathode keeper, cathode heater, and electromagnetic coils. The cathode is kept at chamber potential (ground). Measurements of

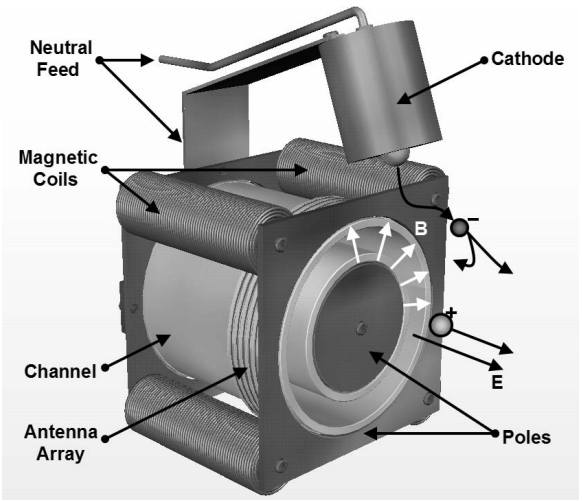

FIG. 1. Diagram of the Stanford Hall Thruster including the antenna diagnostic. The antenna are numbered 1–6 starting from the pole plane.

the discharge current are made using a powered differential amplifier (Tektronix P5200) in parallel with a 4Ω ballast.

B. Nonintrusive antenna diagnostics

Apart from being nonintrusive, a loop antenna diagnostic offers several interesting features that make it ideal for experiments: wide bandwidth, high gain, and a low level of complexity. As a consequence, loop antenna have been used in prior Hall discharge studies to estimate the total azimuthal drift current and its apparent "center of gravity" [12,13]. In the present study the antenna diagnostic is extended so it allows the distribution of the azimuthal drift current to be determined in addition to the drift's "center of gravity."

For this study an antenna array with six closely spaced loops is used. Each loop is a 0.5 mm diameter insulated copper magnet wire connected to a matching 50Ω cable with BNC termination. The antenna array is placed around the discharge channel's outer ceramic wall with the help of a guiding Teflon sleeve. Six holding tracks are cut in the sleeve at 1.6 mm increments. The entire assembly (sleeve and antenna) is thinly coated with a boron nitride spray for electrical and thermal insulation, and one end of the sleeve is polished so it can be positioned next to the magnetic pole at the exit plane with good accuracy (better than 0.1 mm). The placement of the antenna array is shown in Fig. 1.

Fast current interruption of the discharge is achieved using a device similar to the one described by Prioul *et al.* [14]. A power MOSFET in series with the anode is controlled using floating CMOS logic components triggered by a mechanical switch. Using this approach current commutation is obtained in ~200 ns, ~6 times faster than the characteristic time of plasma relaxation (as estimated by line of sight emission measurements in a similar Hall-effect thruster [14]). The simultaneous measurement of the response of each antenna is captured using two digital oscilloscopes (a Tektronix TDS 3014 and a Tektronix TDS 3054) that are simultaneously triggered at the onset of current interruption by the steep decay in the discharge current.

TABLE I. The transfer function for the numerical and experimental calibration techniques for loops 1–6 at two frequencies. Units are V s/A.

Frequency	Test	1	2	3	4	5	6
10 kHz	Num.	4.01	4.51	3.89	4.23	3.68	3.87
10 kHz	Expt.	3.90	4.43	3.90	4.22	3.80	4.01
10 MHz	Num.	0.38	0.84	0.74	1.15	9.43	1.23
10 MHz	Expt.	0.42	0.84	0.76	1.14	9.25	1.25

C. Magnetic field simulation and antenna calibration

The vacuum magnetic field (i.e., the field generated by the thruster's magnetic circuit with no discharge) is simulated with FEMM4.0, a commercially available two-dimensional (2D) finite element software package. Very good agreement (less than 5% difference) is found between the simulation of the magnetic field and measurements of **B** made with a Hall probe (as reported in Ref. [6]).

The same software package is used to calibrate the antenna array by simulating the response of each loop antenna to an arbitrary oscillation of the azimuthal drift current. A distribution of current elements is added to the geometry (varying in spatial position and frequency) and the induced EMF on each antenna is calculated. In this way, one can precisely determine the transfer function of the antenna array, G, which appears when Faraday's law is applied to the axisymmetric model:

$$\delta V(\mathbf{X},\mathbf{x},\omega) = -G(\mathbf{X},\mathbf{x},\omega) i\omega J_\theta(\mathbf{x},\omega)\delta A(\mathbf{x}). \quad (1)$$

Here, δV is the element of EMF induced in a loop at position $\mathbf{X}$ by an element of azimuthal current J_θ at position $\mathbf{x}$, oscillating at frequency ω, with a cross-section given by δA. $\mathbf{X}/\mathbf{x}$ are 2D position vectors in the axial-radial plane. Throughout the present study δA is 1 mm^2.

It is expected that the self-inductances and the interactions between the various current loops in the system (antenna, thruster magnetic circuit, etc.) are negligible, and that induction in the thruster's magnetic circuit is low enough that saturation of the iron core does not occur (thus avoiding the nonlinear mixing of the current frequency modes). This is confirmed using the results of Sec. III.

The accuracy of the numerical calibration procedure is verified by comparing simulations with experimental tests, where a loop antenna is placed inside the thruster discharge chamber and excited with sinusoidal currents at various frequencies. Again, very good agreement between simulations and measurements is found (see Table I). Finally, several tests of the antenna diagnostic were constructed, including various levels of noise. From the results of these tests the accuracy of the loop antenna diagnostic is estimated to be better than 15% at determining the total Hall current, and accurate to a few mm in the placement of the azimuthal drift current's "center of gravity." This error is due to a weak dependence of induced voltage on $\mathbf{x}$, and the choice of $\delta A = 1$ mm^2.

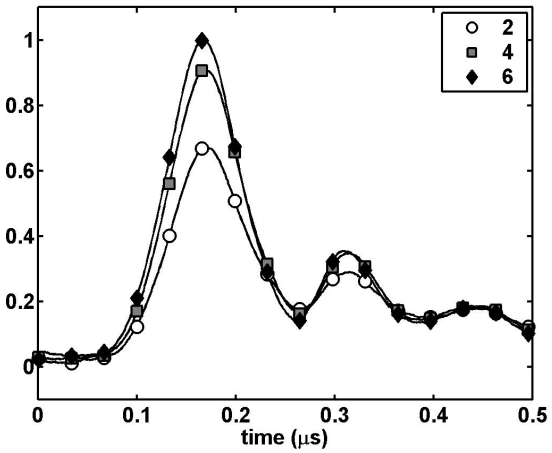

FIG. 2. Representative antenna response.

III. RESULTS AND ANALYSIS

A. The azimuthal drift current

A typical plot of the antenna response to a fast current interruption event is shown in Fig. 2. It is always observed the greatest voltage corresponds to the loop farthest from the exit plane (i.e., loop number 6, see Figs. 1 and 2), and smaller voltages correspond to closer antenna.

In order to reconstruct the original Hall current we assume its spatial distribution and time evolution are independent, i.e., the azimuthal current can be written as

$$J_\theta(\mathbf{x},t) = I_\theta S(\mathbf{x}) T(t). \tag{2}$$

Here, I_θ is the total azimuthal current, S is its spatial distribution, and T is its temporal dependence. It is difficult to evaluate the validity of this assumption since it strongly relates to transport mechanisms in the cross-field discharge. To date, the best verification we have done is to examine the results of a 2D (radial-longitudinal) simulation done by Allis *et al.* [15] at 200 V discharge (one of the discharge conditions we later investigate). Figure 3(a) shows a time average map of the simulated Hall current which is very similar to our experimental results (as we will show). The simulation was run over several milliseconds to collect data on the azimuthal drift current.

To determine the validity of Eq. (2) we introduce the position-dependent function,

$$s = \left\langle \left(\frac{\dfrac{J_\theta(\mathbf{x},t)}{\langle J_\theta(\mathbf{x},t)\rangle_t} - \left\langle \dfrac{J_\theta(\mathbf{x},t)}{\langle J_\theta(\mathbf{x},t)\rangle_t} \right\rangle_x}{\left\langle \dfrac{J_\theta(\mathbf{x},t)}{\langle J_\theta(\mathbf{x},t)\rangle_t} \right\rangle_x} \right)^2 \right\rangle_t^{1/2} \tag{3}$$

which represents a measure of the separability of J_θ. s can be thought of as the standard deviation in the error associated with the assumption of Eq. (2). A result of $s=0$ supports the separability of J_θ, whereas $s \sim 1$ would imply J_θ is not separable. Figure 3(b) is a map of s predicted by the 2D simulation. For the domain of interest ($x=-15$ mm to $x=0$ mm) s is

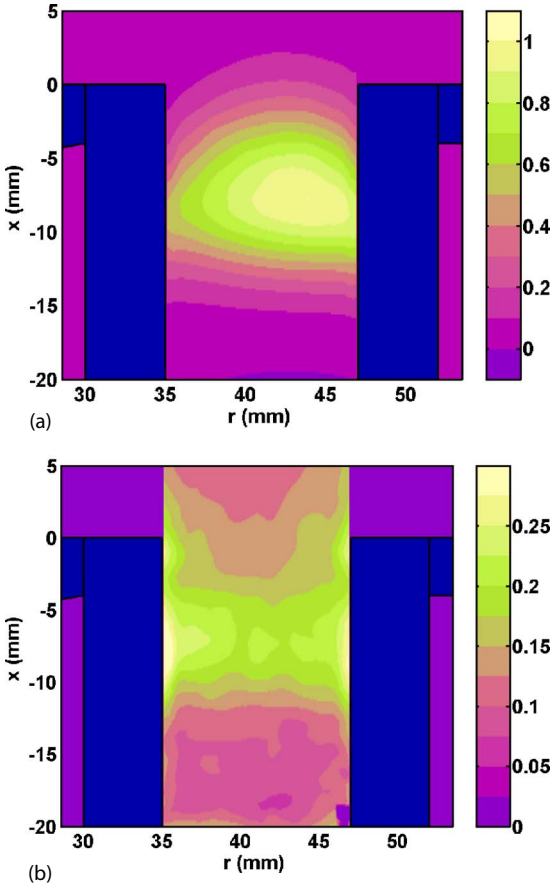

FIG. 3. (Color online) (a) The time-average J_θ simulated by Allis *et al.* [15] at 200 V. (b) The standard deviation in J_θ. Both are normalized. The channel exit is at $x=0$ mm.

less than 0.25. As a consequence, the separation of space and time in Eq. (2) is believed to be reasonable.

Regarding the spatial distribution function $S(\mathbf{x})$, previous measurement made by Bugrova *et al.* [16] with electrostatic probes indicate S can be approximated by a double Gaussian,

$$S(\mathbf{x}) = \frac{1}{2\pi\sigma_r\sigma_x} \exp\left(-\frac{(r-r_c)^2}{2\sigma_r^2} - \frac{(x-x_c)^2}{2\sigma_x^2} \right). \tag{4}$$

Using Eq. (2) and Eq. (4), Eq. (1) can be rewritten as

$$\sum_{r,x} \delta V(\mathbf{X},r,x,\omega) = -I_\theta \delta A \left(\frac{i\omega T(\omega)}{2\pi\sigma_r\sigma_x} \right) \sum_{r,x} G(\mathbf{X},r,x,\omega) \times \exp\left(-\frac{(r-r_c)^2}{2\sigma_r^2} - \frac{(x-x_c)^2}{2\sigma_x^2} \right). \tag{5}$$

The left-hand side of this equation can be calculated from the antenna signals. In the right-hand side the unknowns are the constant parameters σ_r, σ_z, r_c, z_c, I_θ, and the unknown function $T(\omega)$. These unknowns are first estimated using the results from Ref. [16], and the best global fit of these parameters is calculated by iteration using a steepest descent algorithm.

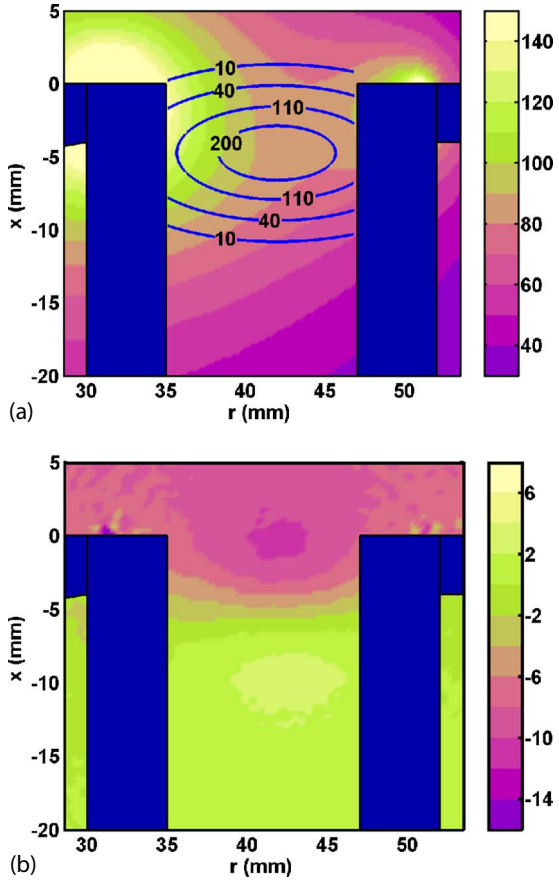

FIG. 4. (Color online) Antenna measurements at 160 V. (a) J_θ in kA/m^2 (contours), and $|\mathbf{B}|$ in Gauss (map). (b) $|\Delta\mathbf{B}|$ in %.

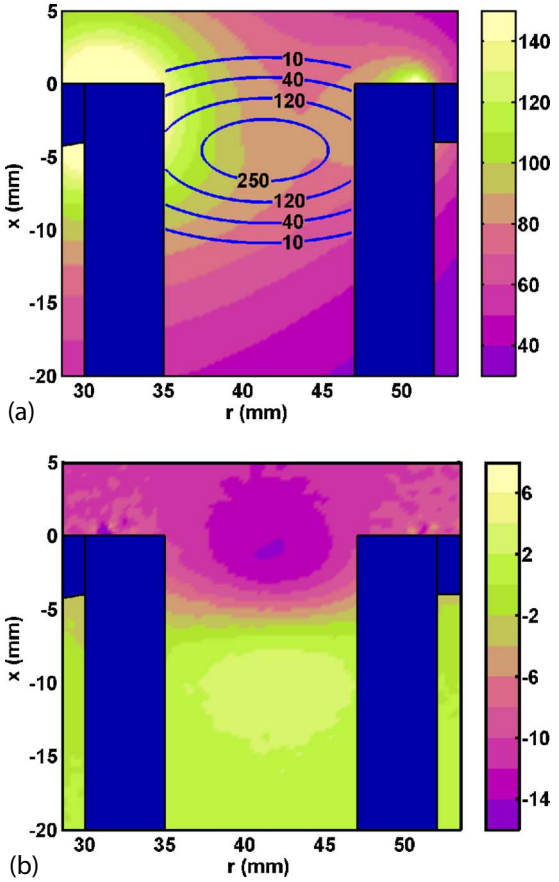

FIG. 5. (Color online) Antenna measurements at 200 V. (a) J_θ in kA/m^2 (contours), and $|\mathbf{B}|$ in Gauss (map). (b) $|\Delta\mathbf{B}|$ in %.

Four tests were carried out with the SHT at 160 V and four more tests at 200 V. At 160 V the average Hall current in the SHT varied little from its average value, 12.5 A. The standard deviation in the drift current over the four tests is 2.2 A, and the time-average discharge current for each test is 1.48 A. The azimuthal drift current and the magnitude of the total magnetic field are shown in Fig. 4(a), and the change in the magnetic field (due to self-induction) is shown in Fig. 4(b).

The maximum drift is located near the maximum magnetic field in vacuum—as expected from classical diffusion theory. The maximum total magnetic field is located near the exit plane (since this is where the poles of the magnetic circuit are located) and is greater on the inner radius (due to the gradient in B common to axisymmetric Hall accelerators, $\nabla\cdot\mathbf{B}=0$). It is apparent in Fig. 4(b) self-induction reduces the magnetic field for axial positions after the exit plane and increases it elsewhere. This results in a shift of the peak total magnetic field toward the anode—an effect detailed more precisely in the next section—and supports the finding that the magnetic field is perturbed from its vacuum value during normal operation, but perhaps not to the extent seen in Ref. [17].

At 200 V the average Hall current is calculated to be 19.2 A. The standard deviation in the four tests is 4.5 A. It is uncertain whether the greater spread at 200 V is due to the small sample size or due to enhanced fluctuations in the azimuthal drift at increased discharge voltage. Previous tests suggest the latter [18]. The time-averaged discharge current for each test is 1.9 A. The azimuthal drift current and the magnitude of the magnetic field are shown in Fig. 5(a), and the change in the magnetic field (due to self-induction) is shown in Fig. 5(b).

At 200 V the drift current is significantly larger than at 160 V, though its radial and axial halfwidth are approximately equal as well as its general location. It should be noted the error in the drift's "center of gravity" obscures any offset in the findings for Figs. 4(a) and 5(b). It is apparent that at 200 V that the maximum magnetic field is again depressed with respect to its vacuum value and shifted towards the anode. These effects are stronger than at 160 V, since the Hall current at 200 V is ~50% greater. As a final note regarding the results of this section, it is observed that the magnetic field perturbation due to the drift current is seen to affect the local magnetic field direction, and appears to do so most markedly at the exit plane. If the magnetic field contours are taken to be electrostatic equipotentials (since electrons move easily along the magnetic field but not across it) the results of this study suggest that including the drift current in the calculation of the magnetic field may shift the magnetic field contours such that the electric field vector near the exit plane of the SHT points more sharply toward

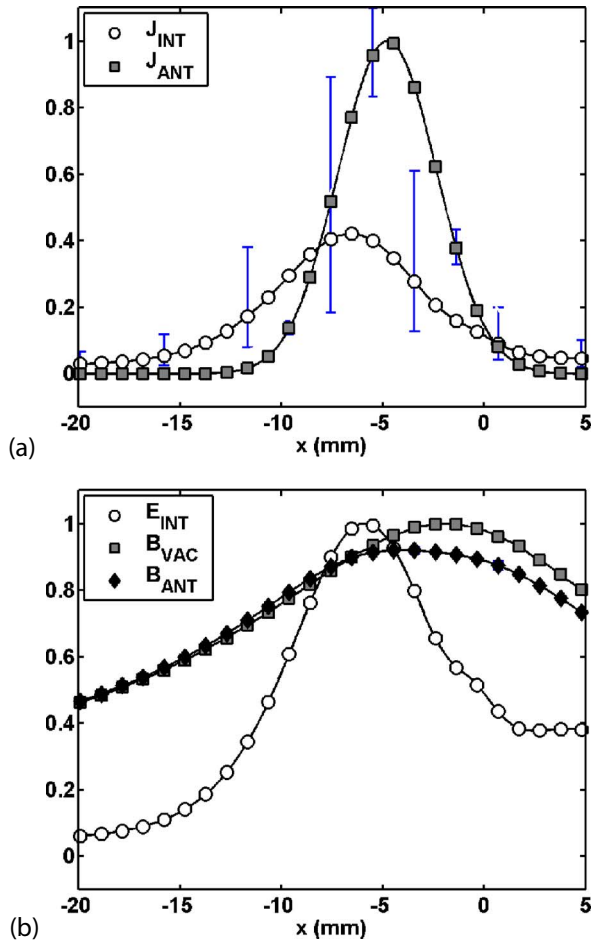

FIG. 6. (Color online) Intrusive, nonintrusive, and vacuum measurements at 160 V. (a) A comparison of the intrusive and nonintrusive J_θ. (b) The relative location of the intrusive **E**, the vacuum $|\mathbf{B}|$, and the nonintrusive $|\mathbf{B}|$.

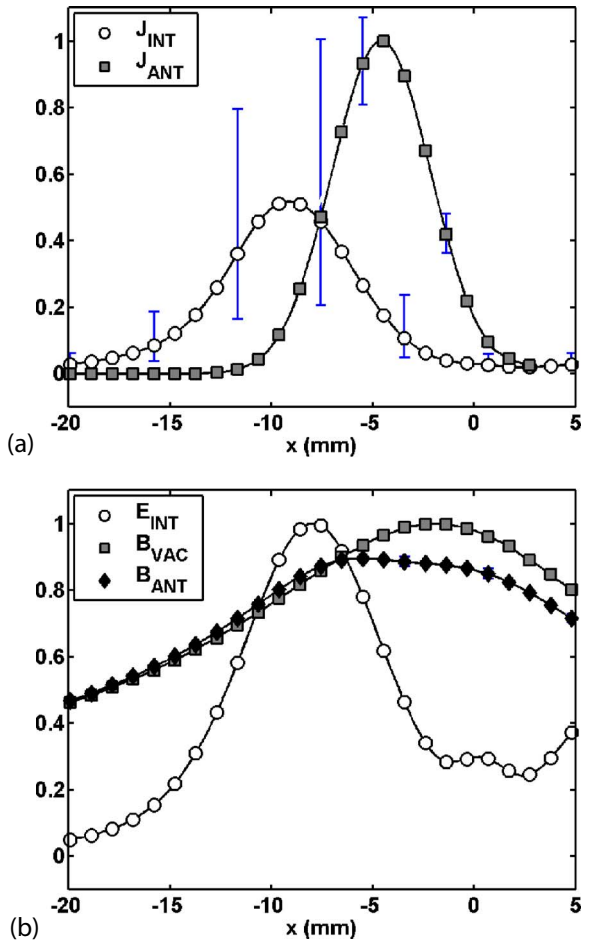

FIG. 7. (Color online) Intrusive, nonintrusive, and vacuum measurements at 200 V. (a) A comparison of the intrusive and nonintrusive J_θ. (b) The relative location of the intrusive **E**, the vacuum $|\mathbf{B}|$, and the nonintrusive $|\mathbf{B}|$.

the discharge channel. This could cause increased sputtering near the exit plane due to increased ion bombardment. More study is needed to quantify the importance of this effect.

B. Center-radius values

To provide a closer examination of the axial field topology within an operating Hall accelerator important values for the azimuthal drift current, magnetic field, and electric field are provided at the center-radius for 160 V and 200 V in Figs. 6(a) and 7(b), respectively.

Discounting small position registration errors ($\sim$2–3 mm) and similar numerical errors in the nonintrusive estimate of azimuthal drift current, it is concluded that the peak in the electric field, radial magnetic field including self-induction, and azimuthal drift are colocated within measurement accuracy. It is also noted that the peak value of the vacuum magnetic field is too near the exit plane, and self-induction shifts the peak in the magnetic field towards the anode so it more closely coincides with the peak electric field. As a result, it can be reasonably concluded that the location of the peak vacuum magnetic field is not an accurate predictor of the location of the peak electric field, nor of the smallest cross-field diffusion coefficient. As a result, it is suggested that numerical simulations of the Hall accelerator should include the azimuthal drift contribution to the magnetic field if possible, since the location of the peak magnetic field is important to the overall resistance of the discharge and the precise location of the ion acceleration zone.

The intrusive and nonintrusive measurements of the azimuthal drift current density agree closely in half-width but differ in magnitude by a factor of $\sim$2. They also display a slight offset in their spatial position. As previously stated, it is expected that the nonintrusive measurement of the azimuthal drift current reported here is accurate to $\sim$15%. The intrusive estimate of the azimuthal drift current in this study is expected to be less accurate, and a reexamination of the data in Ref. [7] suggests it may be in error by a factor of 0.4–2.2. This is certainly consistent with the observed discrepancy between the intrusive and nonintrusive estimate of the azimuthal drift current—especially when it is considered that the ratio of the maximum drift of both methods is consistently off by a factor of $\sim$2 (implying a systematic error). It is therefore concluded that within the level of error, the intrusive estimate of the azimuthal drift current—based on probe-measurements of the plasma potential and electron

number density—agrees with the antenna measurement. As a result, general conclusions regarding the azimuthal drift current in the Hall thruster arrived at using an intrusive estimate of the drift current are believed to be accurate. Of course, the results may also imply the measured electron density or gradient in the plasma potential described in Ref. [6] could be too low by a factor as high as 2. Interestingly, recent simulations of the SHT suggest the likelihood of an error in the plasma potential [15].

Last, it should be noted that the electric field in Ref. [6] used to estimate the intrusive azimuthal current is the primary reason for the spatial offset of the intrusive and nonintrusive azimuthal current [as seen in Figs. 6(a) and 7(a)]. In Ref. [6] a second electric field profile is provided, as inferred from LIF measurements of the ion velocity. The LIF-inferred electric field is shifted 3–5 mm to the right of the intrusively measured electric field. If this **E** is used to estimate the azimuthal drift current in the SHT instead, there is *no* spatial offset in comparison with the antenna measurement. This suggests intrusive plasma property measurements may obscure the precise location of the acceleration and ionization zone (by a few mm) and subtle features that characterize them. The importance of this observation is uncertain, but it does suggest nonintrusive measurements of the plasma properties in the SHT could lead to an improved understanding of HET operation.

IV. SUMMARY

The technique of fast current interruption is combined with an external antenna array to investigate the azimuthal drift current in a Hall accelerator, a coaxial $\mathbf{E}\times\mathbf{B}$ discharge plasma. The distribution of the azimuthal drift current is determined nonintrusively, compared to an intrusive estimate of the azimuthal drift current, and found to agree quantitatively with Ref. [6] (within the level of error estimated for both approaches). As a consequence, it is believed that intrusive estimates of the azimuthal drift are useful for understanding the azimuthal drift current in the HET, though they may be inaccurate at predicting the magnitude of the Hall current. The perturbation to the magnetic field affected by including the azimuthal drift current is then calculated for the SHT at 160 V and 200 V operation. It is found that the drift current magnetic field perturbation caused by the average azimuthal drift shifts the point of the maximum magnetic field in the SHT so it more closely aligns with the maximum **E**. It also depresses the magnitude of the peak magnetic field by 10%–15% (for the operating conditions investigated). Though this may not appear dramatic, it does suggest future numerical models should include the perturbation in the magnetic field caused by the fluctuating azimuthal drift. The precise location of the minimum electron mobility is important to determining the overall resistance of the discharge, and in determining the precise location of the ion acceleration zone (which is important to thrust efficiency and high-energy ion sputtering of the discharge channel).

ACKNOWLEDGMENTS

Funding for this research was provided by the Air Force Office of Scientific Research. One of the authors (N.G.) received financial support from the European Space Agency. One of the authors (C.T.) received support from the National Science Foundation and Stanford University, through the Stanford University Graduate Program. Special thanks is extended to M. Allis [15] for her contribution of simulation results.

[1] V. Zhurin, H. Kaufman, and R. Robinson, Plasma Sources Sci. Technol. **8**, R1 (1999).
[2] G. Janes and R. Lowder, Phys. Fluids **9**, 1115 (1966).
[3] G. Hagelaar, J. Bareilles, L. Garrigues, and J. Boeuf, J. Appl. Phys. **93**, 67 (2003).
[4] J. Fife, Ph.D. thesis, Massachusetts Institute of Technology, 1998.
[5] A. Bishaev and V. Kim, Tech. Phys. **23**, 9 (1999).
[6] W. Hargus, Ph.D. thesis, Stanford University, 2001.
[7] N. Meezan, W. Hargus, and M. Cappelli, Phys. Rev. E **63**, 026410 (2001).
[8] D. Bohm, E. Burhop, and H. Massey, *The Characteristics of Electrical Discharges in Magnetic Fields* (McGraw-Hill, New York, 1949), p. 13.
[9] N. B. Meezan and M. A. Cappelli, Phys. Rev. E **66**, 036401 (2002).
[10] N. Meezan, Ph.D. thesis, Stanford University, 2002.
[11] S. Barral, K. Makowski, Z. Peradzynski, N. Gascon, and M. Dudeck, Phys. Plasmas **10**, 4137 (2003).
[12] V. Dem'yanenko, I. Zubkov, S. Lebedev, and A. Morozov, Sov. Phys. Tech. Phys. **23**, 376 (1978).
[13] A. Bugrova, V. Versotskii, and V. Kharchevnikov, Sov. Phys. Tech. Phys. **25**, 1307 (1980).
[14] M. Prioul, A. Bouchoule, S. Roche, L. Magne, D. Pagnon, and P. Lasgorceix, IEPC Paper No. 01-059, *Proceedings of the International Electric Propulsion Conference* (The Electric Rocket Propulsion Society, Worthington, OH, 2001), IEPC-2001-059.
[15] M. Allis, N. Gascon, M. Cappelli, and E. Fernandez, *40th Joint Propulsion Conference* (American Institute of Aeronautics and Astronautics, Washington, DC, 2004), AIAA-2004-3951.
[16] A. Bugrova, A. Desyatskov, and A. Morozov, Sov. Phys. Tech. Phys. **30**, 610 (1985).
[17] P. Peterson, A. Gallimore, and J. Haas, Phys. Plasmas **9**, 4354 (2002).
[18] C. Thomas, N. Gascon, and M. Cappelli, *39th Joint Propulsion Conference* (American Institute of Aeronautics and Astronautics, Washington, DC, 2004), AIAA-2003-4854.